IPPP/16/17

Interpreting 750 GeV Diphoton Excess in Plain NMSSM

M. Badziak[a,b], M. Olechowski[a], S. Pokorski[a] and K. Sakurai[c]

[a] *Institute of Theoretical Physics, Faculty of Physics, University of Warsaw*
ul. Pasteura 5, PL–02–093 Warsaw, Poland
[b] *Berkeley Center for Theoretical Physics, Department of Physics,*
and Theoretical Physics Group, Lawrence Berkeley National Laboratory,
University of California, Berkeley, CA 94720, USA
[c] *Institute for Particle Physics Phenomenology, Department of Physics,*
University of Durham, Science Laboratories, South Road, Durham, DH1 3LE, UK

arXiv:1603.02203v2 [hep-ph] 4 Jul 2016

Abstract

NMSSM has enough ingredients to explain the diphoton excess at 750 GeV: singlet-like (pseudo) scalar (a) s and higgsinos as heavy vector-like fermions. We consider the production of the 750 GeV singlet-like pseudo scalar a from a decay of the doublet-like pseudo scalar A, and the subsequent decay of a into two photons via higgsino loop. We demonstrate that this cascade decay of the NMSSM Higgs bosons can explain the diphoton excess at 750 GeV.

1 Introduction

Recently ATLAS and CMS have reported excesses in the diphoton mass distribution around $m_{\gamma\gamma} \simeq 750$ GeV in their 13 TeV data. The local significance assuming narrow width is $\sim 3.6\,\sigma$ for ATLAS [1] and $\sim 2.6\,\sigma$ for CMS [2]. ATLAS and CMS have presented their updated analyses at Moriond conference. With the improved analyses, the local significance has increased to $\sim 3.9\,\sigma$ and $\sim 3.4\,\sigma$ for ATLAS and CMS, respectively [3, 4]. Fitting that excess with a narrow resonance around 750 GeV, CMS reports for the cross section times branching ratio, $\sigma_{13\text{TeV}} \cdot \text{BR}_{\gamma\gamma}$, the value $2.6 \div 7.7$ fb at $1\,\sigma$ and $0.85 \div (11-12)$fb at $2\,\sigma$ (see Fig.10 of [4]). The CMS fit of the excess around $m_{\gamma\gamma} \simeq 750$ GeV in the 8 TeV data gives $0.31 \div 1.00$ fb at 1-σ and $0.06 \div 1.45$ fb at 2-σ [4][1]. The ATLAS collaboration has not provided such a detailed analysis for a narrow resonance hypothesis. A fit reported in ref. [5] gives for $\sigma \cdot \text{BR}_{\gamma\gamma}$ the values $\simeq 4 \div 7$ fb and $\simeq 0 \div 0.42$ fb at $1\,\sigma$ at 13 TeV and 8 TeV, respectively. No information about the $2\,\sigma$ regions is available.

The possible interpretation and implications of the excess has been intensively studied. Most such studies introduce new particles to account for the excess without asking about their UV origin, and interpretation within the known models in particular Minimal Supersymmetric Starndard Model (MSSM) and Next-to-Minimal Supersymmetric Standard Model (NMSSM) is rare.[2] In this paper we study the possibility to explain the diphoton excess within the framework of NMSSM without introducing additional particles.

One of the most straightforward interpretations of the excess is to consider a direct production of a scalar or pseudoscalar 750 GeV particle, X, decaying to two photons: $\alpha\beta \to X \to \gamma\gamma$, where α, β are the initial state partons. If the model is renormalizable, $X \to \gamma\gamma$ suggests the existence of electrically-charged vector-like fermions (or scalars) coupled to X [10–68], which generate the effective operator $XF^{\mu\nu}F_{\mu\nu}(\tilde{F}_{\mu\nu})$. Such fermions should be heavier than $m_X/2 \simeq 375$ GeV, otherwise the diphoton rate is strongly suppressed because X predominantly decays into the vector-like fermions on shell. Similar argument disfavours the possibility to identify X as the heavy higgs bosons in the MSSM or 2HDM,[3] because in such models X predominantly decays into $t\bar{t}$ and/or $b\bar{b}$ [71]. In general, in such scenarios the decay branching ratios of X are strongly correlated with the production cross section.

Another possibility is to consider the production of X from a decay of a heavy resonance Y_r associated with another particle Y_d: $\alpha\beta \to Y_r \to Y_d X$, $X \to \gamma\gamma$ [10, 72–75]. This topology has two advantages. First, $\text{BR}(X \to \gamma\gamma)$ is independent of the production cross section of the resonance. This is not the case for the previous topology, because a large production cross section leads to a large rate of the inverse decay process $X \to \alpha\beta$, which suppresses $\text{BR}(X \to \gamma\gamma)$. Second, the mass of Y_r has to be larger than $m_X \simeq 750$ GeV, and the 13

[1] In Fig.10 of [4], CMS rescaled the fitted cross section of the 8 TeV result to 13 TeV assuming the gg initial state. We rescale this back into 8 TeV.

[2] For R-parity violating (RPV) MSSM see [6, 7] and for NMSSM with $pp \to H \to aa \to (\gamma\gamma)(\gamma\gamma)$ see [8, 9].

[3] See however [69, 70].

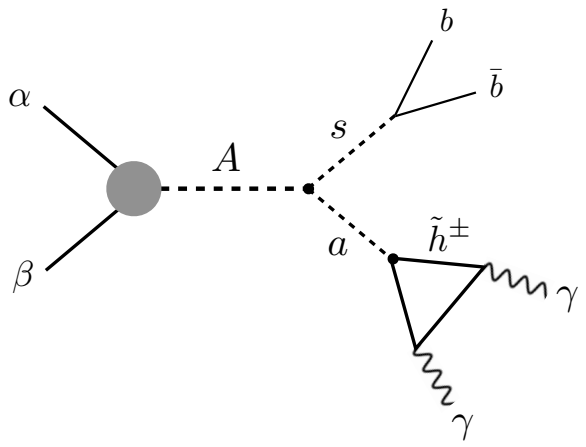

Figure 1: An NMSSM Higgs boson cascade decay contributing to the diphoton excess. The α and β denote the initial state partons. If $(\alpha, \beta) = (b\bar{b})$, one also expects extra b jets in the forward region.

TeV production cross section of Y_r is more enhanced with respect to the 8 TeV cross section, compared to the previous topology. In this context we notice that, while there is no big tension between 8 and 13 TeV data in the CMS fits interpreted as a direct production of a 750 GeV resonance, the fit of ref. [5] to the ATLAS data shows such a tension well above $2\,\sigma$ level. For instance, if the initial partons are gluons, $\alpha\beta = gg$, translating the results of that fit for 8 TeV, interpreted as a direct production of the 750 GeV resonance, to 13 TeV clearly shows the problem. Thus, the cascade topology may slightly help to reconcile the ATLAS data at 8 and 13 TeV and the results of both experiments.

This topology can be relatively easily realised in the NMSSM by identifying $Y_r = A$, $Y_d = s$ and $X = a$: $\alpha\beta \to A \to sa$, $a \to \gamma\gamma$, as shown in Fig. 1, where A is the doublet-like pseudo scalar and (a) s is the singlet-like (pseudo) scalar. In NMSSM $a \to \gamma\gamma$ is induced by a higgsino loop diagram also shown in Fig. 1. The $Y_d = h$ is disfavoured because non-zero Aha coupling requires doublet-singlet mixing in the pseudo-scalar sector (Aa mixing), suppressing $a \to \gamma\gamma$ branching ratio. In our scenario, s predominantly decays into $b\bar{b}$ through a mixing with H. Although the current data would not have enough sensitivity to discriminate these extra jets from other jets with QCD origin, this scenario can be tested by looking at these b-jets in the future analysis.

The paper is organised as follows. In section 2 we demonstrate our scenario in a simplified framework in which the mixing between singlet and doublet states are ignored. In section 3 we consider how our scenario can be realised in the NMSSM taking the effect of mixing into account. We conclude this paper in section 4.

2 Interpretation with pure states

We first discuss our scenario in a simplified framework where the resonance A is pure doublet state and the lightest CP even and odd Higgs bosons, s and a, are exclusively originated from

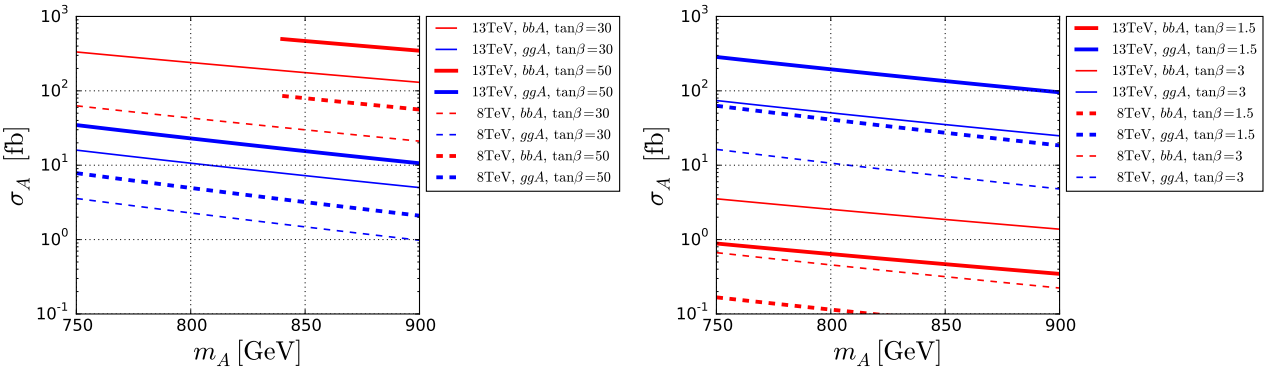

Figure 2: Production cross section of A from the $b\bar{b}$ (red) and gg (blue) initial states as a function of m_A for $\sqrt{S} = 13$ (solid) and 8 (dashed) TeV. In the left (right) panel, the thick and thin lines correspond to $\tan\beta = 50$ and 30 (1.5 and 3), respectively. For the $b\bar{b}$ initial state with $\tan\beta = 50$, $m_A \lesssim 840$ GeV is excluded by the $b\bar{b} \to A \to \tau^+\tau^-$ search.

the singlet field S. The signal of the diphoton excess is given by

$$(\sigma \cdot \mathrm{BR})^{\mathrm{signal}} \equiv \sigma(pp \to A) \cdot \mathrm{BR}(A \to sa) \cdot \mathrm{BR}(a \to \gamma\gamma) \tag{1}$$

where the cross section $\sigma(pp \to A)$ depends on the centre of mass energy of the proton-proton collision.

Fig. 2 shows the NLO production cross section of A from the $b\bar{b}$ (red) and gg (blue) initial states as a function of m_A for $\sqrt{S} = 13$ (solid) and 8 (dashed) TeV. In the left (right) panel of Fig. 2, the thick and thin lines correspond to $\tan\beta = 50$ and 30 (1.5 and 3), respectively. The cross sections are calculated using `SusHi v.1.5.0` [76–83]. As can be seen, the $\sqrt{S} = 13$ TeV production cross section for large (small) $\tan\beta$ values is dominated by $b\bar{b}$ (gg) initial state. It can be as large as 400 (200) fb for $\tan\beta = 50$ (30) at $m_A \sim 850$ GeV. The cross section enhances from 8 TeV to 13 TeV by factor of 5 for gg and 6.7 for $b\bar{b}$ initial states. We impose the m_A dependent upper limit on $\sigma(b\bar{b} \to A) \cdot \mathrm{BR}(A \to \tau^+\tau^-)$ and $\sigma(gg \to A) \cdot \mathrm{BR}(A \to \tau^+\tau^-)$ obtained from the 8 TeV CMS search for the neutral Higgs boson decaying to di-tau [84]. We found the $m_A \lesssim 840$ GeV is excluded by this constraint for $b\bar{b}$ initial state at $\tan\beta = 50$ and this region is not shown in Fig. 2. For $\tan\beta = 30$ or the gg initial state, the whole region with $m_A > 750$ GeV is allowed.

We define the interaction between A-s-a as

$$\mathcal{L} \supset g_{Asa} A s a \,. \tag{2}$$

With the coupling g_{Asa}, the partial decay rate of $A \to sa$ is given by

$$\Gamma(A \to sa) = \frac{|g_{Asa}|^2}{16\pi m_A} \bar{\lambda}\left(\frac{m_s^2}{m_A^2}, \frac{m_a^2}{m_A^2}\right), \tag{3}$$

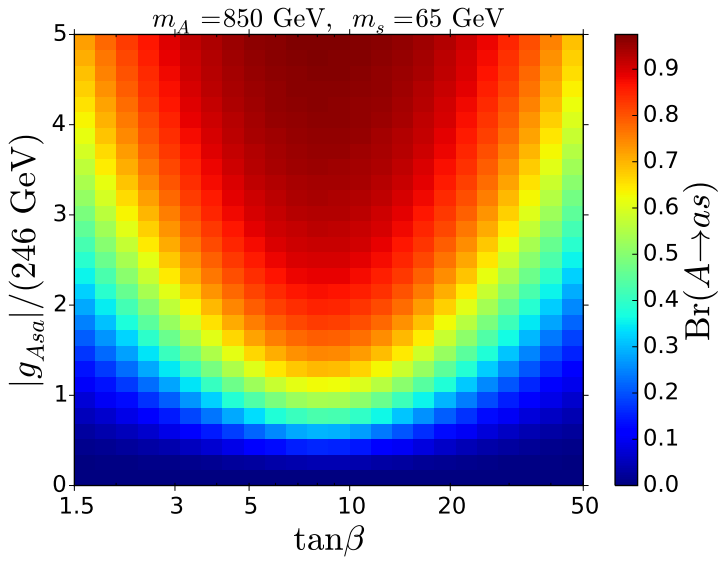

Figure 3: Branching ratio of $A \to sa$ as a function of $\tan\beta$ and $g_{Asa}/(246\,\text{GeV})$. We fix $m_A = 850$ GeV and $m_s = 65$ GeV.

where $\bar{\lambda}(a,b) \equiv 1 + a^2 + b^2 - 2(a + b + ab)$. In what follows we assume $m_s = 65$ GeV and $815 \leq m_A \leq 875$ GeV. In this parameter region, $h \to ss$ and $A \to ha$ are kinematically forbidden while $A \to sa$ is allowed.

The $A \to sa$ decay mode competes with $A \to b\bar{b}$ and $A \to t\bar{t}$ in the large and small $\tan\beta$ regimes, respectively. The partial decay rates are given by

$$\Gamma(A \to b\bar{b}) = \frac{3\alpha_W m_A}{8m_W^2} m_b^2 \tan^2\beta \Big(1 - \frac{4m_b^2}{m_A^2}\Big)^{1/2}, \quad \Gamma(A \to t\bar{t}) = \frac{3\alpha_W m_A}{8m_W^2} m_t^2 \cot^2\beta \Big(1 - \frac{4m_t^2}{m_A^2}\Big)^{1/2}. \tag{4}$$

The decay modes into gauge bosons are highly suppressed due to the CP property. Fig. 3 shows the branching ratio of $A \to sa$ for $m_A = 850$ GeV, $m_s = 65$ GeV as a function of $\tan\beta$ and $|g_{Asa}|/(246\,\text{GeV})$. At a fixed g_{Asa}, BR$(A \to sa)$ is maximised around $\tan\beta \sim 7$. This is because the decay rate of $A \to f\bar{f}$ is minimised in this region. For small ($\lesssim 2$) and large ($\gtrsim 30$) $\tan\beta$, $|g_{Asa}|/(246\,\text{GeV}) \gtrsim 1.5$ is required to have BR$(A \to sa) \gtrsim 0.3$.

We focus on the process in which a decays to two photons through higgsino loop.[4] If a is pure singlet and the gauginos are decoupled, BR$(a \to \gamma\gamma)$ does not depend on the higgsino mass nor the $a\tilde{h}^+\tilde{h}^-$ coupling, and is entirely determined by quantum numbers of higgsinos. The branching ratios are given as

$$\text{BR}(a \to W^+W^-) \approx 0.65, \quad \text{BR}(a \to ZZ) \approx 0.23, \quad \text{BR}(a \to \gamma Z) \approx 0.05, \quad \text{BR}(a \to \gamma\gamma) \approx 0.07. \tag{5}$$

We now combine the cross section and branching ratios to see if the model can fit the 13 TeV excess consistently with the 8 TeV data. Since the CMS detailed data analysis and the

[4] Similar idea has been discussed [85] in the context of the 125 GeV Higgs boson.

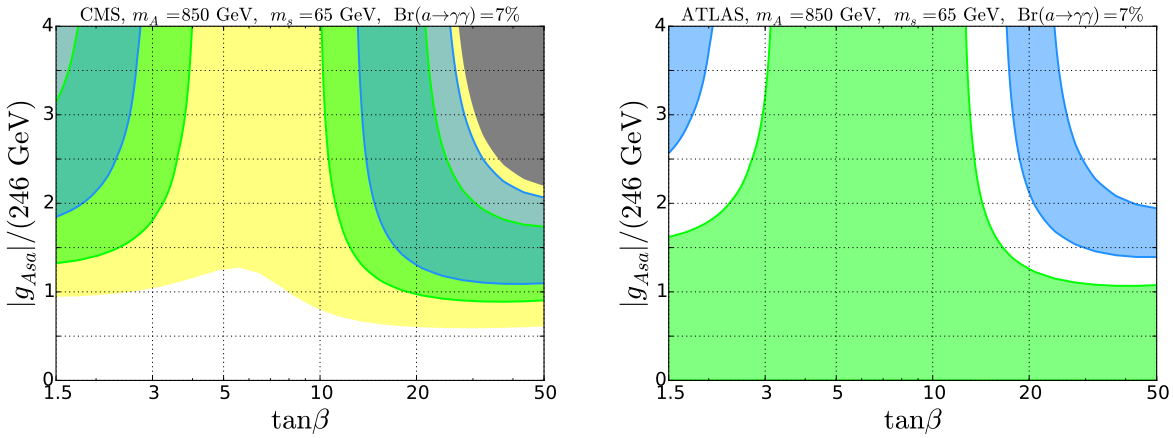

Figure 4: Left: The results for the coupling g_{Asa} as a function of $\tan\beta$ based on the CMS fit. The blue (yellow) region is favoured by the 13 TeV excess at $1\,\sigma$ ($2\,\sigma$) level. The green region is favoured by the excess in the 8 TeV data at $1\,\sigma$ level. (The blue and green regions partly overlap.) The grey region is beyond the 2-σ in the 8 TeV data. Right: The results for the coupling g_{Asa} as a function of $\tan\beta$ based on the fit of ref. [5] to the ATLAS data. The blue region is favoured by the 13 TeV excess at $1\,\sigma$ level. The green region is favoured by the excess in the 8 TeV data at $1\,\sigma$ level.

fit of ref. [5] to the ATLAS data are not on equal footing, we do not average their results and discuss them in turn. The results for the coupling g_{Asa} based on the CMS analysis are summarized in the left panel of Fig. 4. The blue region is favoured by the 13 TeV excess at $1\,\sigma$ level, $(\sigma\cdot\mathrm{BR})^{\mathrm{signal}}_{13\mathrm{TeV}} \in [2.6,\ 7.7]$ fb, and the yellow one by the $2\,\sigma$ range [0.85, 12] fb. The green region is favoured by the excess in the 8 TeV data at $1\,\sigma$ level, $(\sigma\cdot\mathrm{BR})^{\mathrm{signal}}_{8\mathrm{TeV}} \in [0.31,\ 1.00]$ fb. The grey region corresponds to $(\sigma\cdot\mathrm{BR})^{\mathrm{signal}}_{8\mathrm{TeV}} > 1.45$ fb which is disfavoured at 2-σ at 8 TeV.

As can be seen, there exist two favoured regions, (a) small ($\lesssim 2$) $\tan\beta$ region and (b) large ($\gtrsim 20$) $\tan\beta$ region. This is because the production cross section, $pp\to A$, is maximised for these two regions. In the small $\tan\beta$ region $gg\to A$ via the top-quark loop dominates the production processes, whereas $b\bar{b}\to A$ is dominant in the large $\tan\beta$ region. The enhancement in the cross section compensates the slight suppression in BR($A\to sa$) (see Fig. 3). For moderate $\tan\beta$, the signal event rate cannot be large enough to be within the $1\,\sigma$ regions due to the small cross section even for $|g_{Asa}|/(246\,\mathrm{GeV}) \gtrsim 1.5$ where the BR($A\to sa$) is already saturated BR($A\to sa$) ~ 1 and increasing g_{Asa} further does not help to enhance the signal rate. As can be seen, both favoured regions require relatively large g_{Asa} coupling. For large and small $\tan\beta$ regions, the $1\,\sigma$ region requires $|g_{Asa}|/(246\,\mathrm{GeV}) \gtrsim 1$ and 2, respectively.

In the right panel of Fig. 4 we show the results for the coupling g_{Asa} based on the fit of ref. [5] to the ATLAS data. We see that the tension between the 13 and 8 TeV data does not disappear even with the cascade decay topology, where the primary object has the mass of 850 GeV, and remains at the level of approximately $2\,\sigma$. [5] The excess at 13 TeV requires, at $1\,\sigma$,

[5] In the December ATLAS note [1], it is stated that the 8 and 13 TeV data sets, interpreted as a narrow resonance with mass of 750 GeV and produced from gg initial state, are compatible to each other at 2.2σ. No

somewhat larger values of the coupling g_{Asa}.

In the simplified framework discussed so far, the dominant decay mode of s becomes $s \to \gamma\gamma$ because other gauge boson final states are not kinematically allowed. This will cause a strong tension with the fact that ATLAS and CMS did not observe extra photons other than the diphoton excess with $m_{\gamma\gamma} \simeq 750$ GeV. However, this problem can be easily circumvented by introducing a mixing between s and H. With this mixing s will dominantly decay into $b\bar{b}$.

3 Realisation in NMSSM

The superpotential and soft SUSY breaking Lagrangian of the NMSSM are given by (c.f. [86])

$$W = W_{\rm MSSM} + \lambda S H_u H_d + \xi_F S + \frac{1}{2}\mu' S^2 + \frac{\kappa}{3} S^3 \,, \tag{6}$$

$$-\mathcal{L}_{\rm soft} = -\mathcal{L}_{\rm soft}^{\rm MSSM} + m_S^2 |S|^2 + \left[\lambda A_\lambda S H_u H_d + \frac{1}{3}\kappa A_\kappa S^3 + \frac{1}{2} m_3'^2 S^2 + \xi_S S + {\rm h.c.}\right], \tag{7}$$

where we assume all couplings are real.[6] Notice that the MSSM μ-term, $W_{\rm MSSM} \supset \mu_{\rm MSSM} H_u H_d$, can be removed by redefining S by a constant shift. We fix S in this way, hence $\mu_{\rm MSSM} = 0$. We first rotate the doublet Higgs bosons H_u and H_d by the angle β and define the new field basis

$$\hat{H} = \sin\beta H_{dR}^0 - \cos\beta H_{uR}^0 \,, \quad \hat{h} = \cos\beta H_{dR}^0 + \sin\beta H_{uR}^0 \,, \quad \hat{s} = S_R \,, \tag{8}$$

$$\hat{A} = \sin\beta H_{dI}^0 + \cos\beta H_{uI}^0 \,, \quad \hat{G} = \cos\beta H_{dI}^0 - \sin\beta H_{uI}^0 \,, \quad \hat{a} = S_I \,. \tag{9}$$

By this rotation, $\hat{H}$ does not have the vacuum expectation value, and $\hat{G}$ becomes the Goldstone boson eaten by Z. The scalar mass eigenstates, denoted by h_i (with $h_i = h, H, s$ where h is the SM-like Higgs), are expressed in terms of the hatted fields with the help of the diagonalization matrix $\tilde{S}$:

$$h_i = \tilde{S}_{h_i \hat{h}} \hat{h} + \tilde{S}_{h_i \hat{H}} \hat{H} + \tilde{S}_{h_i \hat{s}} \hat{s} \,. \tag{10}$$

The pseudoscalar mass eigenstates, A and a, are related to the hatted fields, $\hat{A}$ and $\hat{a}$, by a rotation by angle θ_{Aa}.

The $\hat{A}$-$\hat{s}$-$\hat{a}$ interaction is given by the F-term of S as $|\frac{\partial W}{\partial S}|^2 \supset \lambda\kappa H_u H_d S^* S^* \supset -v_{\rm SM} \lambda\kappa \hat{A}\hat{s}\hat{a}$, where $v_{\rm SM} = 246$ GeV. In the previous section we mentioned that one should allow the $\hat{H}$-$\hat{s}$

update for this number has been given after Moriond conference and one cannot infer it from the fit of ref. [5]. We note that for 850 GeV resonance produced from $b\bar{b}$ initial state the increase of the cross-section from 8 to 13 TeV is about 40% bigger than that for 750 GeV resonance produced from gg initial state. In the right panel of Fig. 4 we see that, indeed, the compatibility between the fits of ref. [5] to 8 and 13 TeV data sets is somewhat better at large $\tan\beta$ than at its small values.

[6] We use general NMSSM Lagrangian without imposing Z_3 or scale invariance. This version of NMSSM has various phenomenological advantages. See e.g. [87, 88].

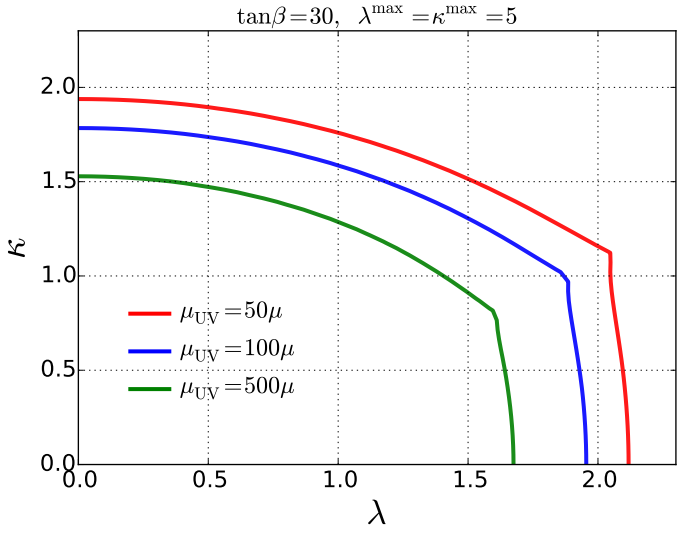

Figure 5: The limit for the Landau pole constraint. At the green (blue and red) contour $\max[\lambda(\mu_{\rm UV}), \kappa(\mu_{\rm UV})] = 5$, where $\mu_{\rm UV} = 500\mu$, $(100\mu,\ 50\mu)$.

mixing in order to suppress unwanted $s \to \gamma\gamma$ decay. Neglecting A-a mixing, the coupling g_{Asa} is given as

$$g_{Asa}/v_{\rm SM} = -\lambda\kappa\tilde{S}_{s\hat{s}}\,. \tag{11}$$

In the previous section we have shown that $|g_{Asa}/v_{\rm SM}| \gtrsim 1$ (2) is required for $\tan\beta \gtrsim 20$ ($\lesssim 2$) (See Fig. 4.). Clearly, one needs the product $|\lambda\kappa| \gtrsim 1$ (2) for large (small) $\tan\beta$ to explain the excess. Such large values of λ and/or κ indicate the Landau pole at the scale $\mu_{\rm UV}$ much below the GUT scale. In Fig. 5 we show the constraint from the Landau pole. If our topology is responsible for the observed diphoton excess, this indicates the existence of the UV cut-off typically of the order of 100 TeV.

Dropping the Goldstone mode, the entries of the mass matrix for the pseudo-scalar sector (A, a) are given by

$$M^2_{\hat{A}\hat{A}} = \frac{2(\mu B_{\rm eff} + \hat{m}_3^2)}{\sin 2\beta} + \Delta^2_{AA}, \tag{12}$$

$$M^2_{\hat{a}\hat{a}} = \frac{1}{v_s}\left[\frac{\lambda v_{\rm SM}^2 \sin 2\beta}{4}(B_{\rm eff} + \mu') - \xi_F\mu' - \xi_S\right] + \kappa\left[\frac{3\lambda v_{\rm SM}^2 \sin 2\beta}{4} - 4\xi_F\right] - 2m_S'^2 - \kappa v_s(3A_\kappa + \mu') + \Delta^2_{aa}, \tag{13}$$

$$M^2_{\hat{A}\hat{a}} = \frac{\lambda v_{\rm SM}}{\sqrt{2}}(A_\lambda - 2\kappa v_s - \mu') + \Delta^2_{Aa}\,, \tag{14}$$

where $B_{\rm eff} \equiv A_\lambda + \kappa v_s$ and $\hat{m}_3^2 \equiv m_3^2 + \lambda(\mu' v_s + \xi_F)$. The m_3^2 is the soft breaking mass term $\mathcal{L}^{\rm MSSM}_{\rm soft} \supset m_3^2 H_u H_d$, $v_s \equiv \langle s\rangle \equiv \mu/\lambda$ and $\Delta^2_{AA/aa/Aa}$ are the radiative corrections.

The mixing between A and a is determined by

$$\sin 2\theta_{Aa} = \frac{2M^2_{\hat{A}\hat{a}}}{m_A^2 - m_a^2} \simeq \frac{\lambda(A_\lambda - 2\kappa v_s - \mu')}{460\,\mathrm{GeV}} + \frac{\Delta^2_{Aa}}{(283\,\mathrm{GeV})^2}\,, \tag{15}$$

where we used $m_A = 850$ GeV, $m_a = 750$ GeV. This mixing strongly affects the BR($a \to \gamma\gamma$) because it introduces $a \to b\bar{b}$ and $t\bar{t}$ modes through the mixing. The reduction of the signal strength can be parameterized by r as

$$(\sigma \cdot \mathrm{BR})^{\mathrm{signal}} = r \cdot (\sigma \cdot \mathrm{BR})^{\mathrm{signal}}_{\mathrm{pure}}\,. \tag{16}$$

For $|\sin\theta_{Aa}| \ll 1$, r can be written as

$$r = \frac{\cos^2\theta_{Aa}\Gamma^a_{VV}}{\sin^2\theta_{Aa}\Gamma^A_{f\bar{f}} + \cos^2\theta_{Aa}\Gamma^a_{VV}} \tag{17}$$

where $\Gamma^A_{f\bar{f}}$ is the sum of the partial decay rates in Eq. (4) at $m_A = 750$ GeV and Γ^a_{VV} is the sum of the partial decay rates of the pure state a into W^+W^-, ZZ, $Z\gamma$ and $\gamma\gamma$, which can be written as

$$\Gamma^a_{VV} = |\lambda|^2 f(m_{\tilde{h}})\,. \tag{18}$$

The factor $|\lambda|^2$ can be understood because $a\tilde{h}\tilde{h}$ coupling is given by $\frac{\lambda}{\sqrt{2}}$. The $f(m_{\tilde{h}})$ is obtained from the higgsino loop diagram and we find $f(m_{\tilde{h}}) \simeq 1.5 \cdot 10^{-2}$ GeV for $m_{\tilde{h}} = |\mu| \simeq 375$ GeV. The condition $r \gtrsim 0.5$ can be translated as

$$|\tan\theta_{Aa}| \lesssim \Big[\frac{|\lambda|^2 f(m_{\tilde{h}})}{\Gamma^A_{f\bar{f}}}\Big]^{1/2} \sim 0.03\,|\lambda| \tag{19}$$

for large ($\gtrsim 10$) or small ($\lesssim 2$) $\tan\beta$. This puts a strong constraint on the parameters appearing in Eq. (15).

In the scalar sector ($\hat{H}$, $\hat{h}$, $\hat{s}$), the elements of the mass matrix are given by

$$\begin{aligned}
M^2_{\hat{H}\hat{H}} &= M^2_{AA} + (m_Z^2 - \frac{\lambda^2}{2}v^2_{\mathrm{SM}})\sin^2 2\beta + \Delta^2_{HH}, && (20)\\
M^2_{\hat{h}\hat{h}} &= m_Z^2\cos^2 2\beta + \frac{\lambda^2}{2}v^2_{\mathrm{SM}}\sin^2 2\beta + (\delta m_h^2)^{\mathrm{rad}} + \Delta^2_{hh}, && (21)\\
M^2_{\hat{s}\hat{s}} &= \kappa v_s(4\kappa v_s + A_\kappa + 3\mu') + \frac{1}{v_s}\Big[\frac{\lambda v^2_{\mathrm{SM}}\sin 2\beta}{4}(A_\lambda + \mu') - (\mu'\xi_F + \xi_S)\Big] + \Delta^2_{ss}, && (22)\\
M^2_{\hat{H}\hat{h}} &= \frac{1}{2}(m_Z^2 - \frac{\lambda^2}{2}v^2_{\mathrm{SM}})\sin 4\beta + \Delta^2_{Hh}, && (23)\\
M^2_{\hat{H}\hat{s}} &= \frac{\lambda}{\sqrt{2}}v_{\mathrm{SM}}\Lambda\cos 2\beta + \Delta^2_{Hs}, && (24)\\
M^2_{\hat{h}\hat{s}} &= \frac{\lambda}{\sqrt{2}}v_{\mathrm{SM}}(2\mu - \Lambda\sin 2\beta) + \Delta^2_{hs}\,, && (25)
\end{aligned}$$

where $\Lambda \equiv B_{\rm eff} + \kappa v_s + \mu' = A_\lambda + 2\kappa v_s + \mu'$ and $(\delta m_h^2)^{\rm rad}$ is the radiative correction induced by the stop loop. Typically, for large $\tan\beta$ this scenario requires heavy stops ($m_{\tilde{t}} \sim \mathcal{O}(10)$ TeV) depending on the size of the stop mixing parameter X_t in order to achieve $m_h = 125$ GeV. The $\Delta^2_{HH/hh/ss/Hh/Hs/hs}$ are the radiative corrections contributing to the NMSSM Higgs boson mass matrices.

The elements of the diagonalization matrix $\tilde{S}$ must respect various phenomenological constraints. The LEP limit on the $e^+e^- \to Z^* \to Zs$ ($s \to b\bar{b}$) process for the 65 GeV scalar gives the bound $\tilde{S}_{s\hat{h}} \cdot {\rm BR}(s \to b\bar{b}) \lesssim 0.16$ [89], where ${\rm BR}(s \to b\bar{b})$ depends in principle on $\tilde{S}_{s\hat{H}}$ mixing and $\tan\beta$ [90]. The measurements of the properties of the SM-like Higgs boson at the LHC also give constraints on the mixing angles. The deviation of its coupling to the gauge bosons is now constrained up to $\sim 20\,\%$ at $95\,\%$ CL [91, 92]. This translates into the constraint on the $\tilde{S}$ entries as $\tilde{S}_{h\hat{H}}, \tilde{S}_{h\hat{s}} \lesssim 0.2$.

In the parameter space relevant for our model, the elements $\tilde{S}_{s\hat{H}}$ and $\tilde{S}_{H\hat{s}}$ remain unconstrained and may be large. Neglecting the small mixing elements they may be approximated by

$$\tilde{S}_{s\hat{H}} \simeq \sin\theta_{sH} \simeq -\tilde{S}_{H\hat{s}}\,, \tag{26}$$

where for future convenience we introduced the mixing angle θ_{sH} satisfying

$$\sin 2\theta_{sH} = \frac{2M^2_{Hs}}{m_s^2 - m_H^2} \simeq -\frac{\lambda\Lambda\cos 2\beta}{2\,{\rm TeV}} - \frac{\Delta^2_{Hs}}{(600\,{\rm GeV})^2}\,, \tag{27}$$

In the last equality we have used $m_H = 850$ GeV, $m_s = 65$ GeV. The two small off-diagonal entries of $\tilde{S}$ may be approximated as follows

$$\tilde{S}_{s\hat{h}} \simeq \frac{\cos\theta_{sH} M^2_{\hat{h}\hat{s}} + \sin\theta_{sH} M^2_{\hat{H}\hat{h}}}{m_s^2 - m_h^2}\,, \qquad \tilde{S}_{H\hat{h}} \simeq \frac{\cos\theta_{sH} M^2_{\hat{H}\hat{h}} - \sin\theta_{sH} M^2_{\hat{h}\hat{s}}}{m_H^2 - m_h^2}\,. \tag{28}$$

The elements $\tilde{S}_{h\hat{H}}$ and $\tilde{S}_{h\hat{s}}$ are related to the above ones by orthogonality of $\tilde{S}$:

$$\tilde{S}_{h\hat{s}} \simeq -\cos\theta_{sH}\tilde{S}_{s\hat{h}} + \sin\theta_{sH}\tilde{S}_{H\hat{h}}\,, \qquad \tilde{S}_{h\hat{H}} \simeq -\cos\theta_{sH}\tilde{S}_{H\hat{h}} - \sin\theta_{sH}\tilde{S}_{s\hat{h}}\,. \tag{29}$$

Clearly, the values of the Higgs boson masses and the constraints on the mixing angles would select some regions of the NMSSM parameter space. However, the complexity of the NMSSM Higgs potential make a full quantitative analysis of our scenario, with radiative corrections included, challenging and premature. Merely for the illustration purpose, we attempt to find the NMSSM parameters that satisfy the above conditions using approximate forms of the 1-loop radiative corrections. Some attention has to be paid to the magnitude of the radiative corrections. Indeed, we note that some of the 1-loop radiative correction terms are proportional to the 3rd power of λ or κ and can be as large as the tree level terms for $|\lambda|$, $|\kappa| \gtrsim 1$ [93]. The 2-loop corrections may also be large [94] in this region.[7] For large λ and κ, neglecting the

[7] For instance, a brute force parameter scan using numerical tools that include such corrections is computationally very expensive since one has to find a narrow region where the mixing parameters, $\sin\theta_{Aa}$ and $\tilde{S}_{s\hat{h}}$, are small.

corrections proportional to the gauge and Yukawa couplings, the leading terms of the radiative corrections to the off-diagonal mass matrix elements are given by[8]

$$\Delta^2_{Hs} = \frac{\kappa v_{\rm SM}\mu}{8\sqrt{2}\pi^2}\left(2\lambda^2 L_\mu + 2\kappa^2 L_\nu - 3\lambda^2 L_{\mu\nu}\right)\cos(2\beta)\,, \tag{30}$$

$$\Delta^2_{hs} = \frac{\lambda v_{\rm SM}\mu}{8\sqrt{2}\pi^2}\left(2\lambda^2 L_\mu + 2\kappa^2 L_\nu - \left(\lambda^2 + 8\kappa^2\right) L_{\mu\nu}\right) - \Delta^2_{Hs}\tan(2\beta)\,, \tag{31}$$

$$\Delta^2_{Aa} = \Delta^2_{Hh} = 0\,, \tag{32}$$

where

$$L_\mu = \ln\left(\frac{\mu^2}{M_Z^2}\right), \qquad L_\nu = \ln\left(\frac{(2\kappa v_s + \mu')^2}{M_Z^2}\right), \qquad L_{\mu\nu} = \ln\left(\frac{\max(\mu^2, (2\kappa v_s + \mu')^2)}{M_Z^2}\right). \tag{33}$$

It is easy to find solutions for the parameters of the model satisfying the constraints $m_H = m_A = 850$ GeV, $m_s = 65$ GeV , $\mu = 375$ GeV, vanishing Aa mixing ($\theta_{Aa} = 0$) and small $\tilde{S}_{s\hat{h}}$. We used the following procedure: The scalar mass squared matrix has 6 independent parameters. We choose them as 3 eigenvalues (m_h^2, m_H^2, m_s^2) and 3 off-diagonal entries of the diagonalization matrix ($\tilde{S}_{s\hat{H}}$, $\tilde{S}_{s\hat{h}}$, $\tilde{S}_{h\hat{H}}$). Using this parameterization we calculate the off-diagonal elements of the scalar mass squared matrix and compare them with the same elements expressed by the parameters of the model in eqs. (23)-(25). One of the parameters, μ', is fixed by the requirement of vanishing A-a mixing: $\mu' = A_\lambda - 2\mu\kappa/\lambda$. Then, for some fixed values of the elements ($\tilde{S}_{s\hat{H}}$, $\tilde{S}_{s\hat{h}}$, $\tilde{S}_{h\hat{H}}$), we are left with the set of three equations for three parameters: λ, κ and A_λ. In general there is a discrete set of solutions.

In the actual numerical calculations we had to modify this simple prescription. In order to compare our results with the experimental constraints illustrated in Fig. 4 we were fixing the value of g_{Asa} given by eq. (11). This fixes one combination of the parameters λ, κ and A_λ. Thus, only two mixing elements (chosen to be $\tilde{S}_{s\hat{H}}$, $\tilde{S}_{s\hat{h}}$) remain as input for our calculations while the third one ($\tilde{S}_{h\hat{H}}$) is obtained as output. Numerical iteration procedures are used to find solutions.

One of the input mixing elements, $\tilde{S}_{s\hat{h}}$, is quite strongly constrained by the LEP data. Thus, after fixing the values of the scalar masses and $\tan\beta$, $\tilde{S}_{s\hat{H}}$ remains the only input quantity which may be changed in a relatively wide range. The dependence of the results on $\tilde{S}_{s\hat{H}}$ is shown in Fig. 6 for the example with $\tan\beta = 20$, $\tilde{S}_{s\hat{h}} = 0$ and $|g_{Asa}| = 0.6$. One can see that λ increases with $\tilde{S}_{s\hat{H}}$ while $|\kappa|$ has a minimum. The behavior of λ follows from the fact that for bigger mixing $\tilde{S}_{s\hat{H}}$ one needs bigger $M^2_{\hat{H}\hat{s}}$ which grows with λ (at least the tree contribution, see eq. (24)). Then the behavior of κ follows from relation (11). The leading (in λ and κ) loop correction to the Higgs mass is a quite complicated function of the parameters. From the right panel in Fig. 6 one can see that it may even vanish for some combination of λ and κ but generally is an increasing function of the input mixing parameter $\tilde{S}_{s\hat{H}}$. Examples presented in Fig. 6 (and in Table 1) were obtained for $\tilde{S}_{s\hat{h}} = 0$. We checked that the results do not change substantially for the values of $\tilde{S}_{s\hat{h}}$ allowed by the LEP data.

[8] We applied the loop corrections from ref. [93] modified by the Z_3 non-invariant contributions.

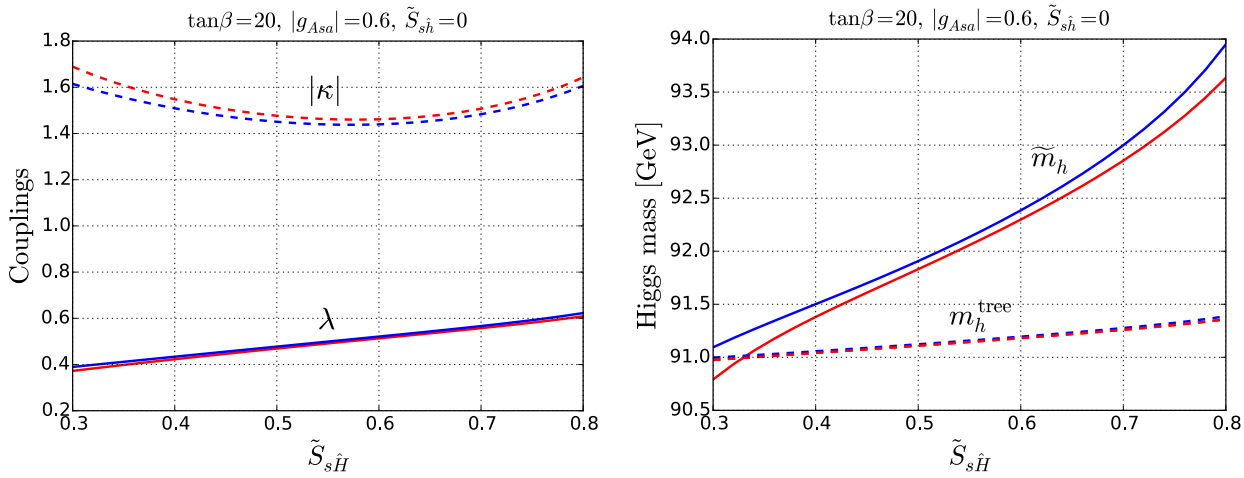

Figure 6: Left panel: λ (solid) and $|\kappa|$ (dashed) as functions of $\tilde{S}_{s\hat{H}}$. Right panel: the SM-like Higgs boson mass at the tree level, $m_h^{\rm tree}$, (dashed) and with the leading (for large λ and κ) loop corrections (but before including the radiative correction from the scalar top loop), $\widetilde{m}_h$, (solid) as functions of $\tilde{S}_{s\hat{H}}$. Solutions with positive (red) and negative (blue) values of κ are shown. Other parameters are fixed at: $\tan\beta = 20$, $|g_{Asa}| = 0.6$, $\tilde{S}_{s\hat{h}} = 0$.

A few generic examples are presented in Table 1. For large $\tan\beta$ the values of $\tilde{S}_{s\hat{H}}$ are chosen to give $|\kappa|$ close to the smallest possible (for a given set of other parameters) value in order to get the Landau pole scale as big as possible. For small $\tan\beta$ we have to choose much smaller $\tilde{S}_{s\hat{H}}$ in order to avoid huge tree level contribution to the Higgs mass (value of λ increases with $\tilde{S}_{s\hat{H}}$). The first example in Table 1 shows that $\tilde{S}_{s\hat{H}} \gtrsim 0.1$ can easily lead to too large $m_h^{\rm tree}$ for $\tan\beta = 2$. The last two columns of Table 1 show the SM-like Higgs boson at the tree level, $m_h^{\rm tree}$, and with the leading (for large λ and κ) loop corrections, $\widetilde{m}_h$ (but before including the radiative correction from the scalar top loop). An interesting observation is that in the parameter range selected by the constraints of very small $\hat{h}$-$\hat{s}$ and $\hat{A}$-$\hat{a}$ mixings the radiative corrections to the Higgs potential from the NMSSM Higgs bosons are actually small, in spite of the sizable values of λ and, particularly, κ. This is related to the fact that some of potentially large contributions are proportional to appropriate mixing elements and are small in the limit of small mixings. Thus, the values of $\widetilde{m}_h$ given in Table 1 are almost entirely controlled by the tree-level effects. The mixing elements, other than $\tilde{S}_{s\hat{H}} \approx -\tilde{S}_{H\hat{s}}$, are small once $\tilde{S}_{s\hat{h}}$ is taken to be small (to fulfill the LEP constrains). $\tilde{S}_{H\hat{h}}$ is suppressed by m_H^2 (see eqs. (28)) and typically is below 0.01. The two remaining off-diagonal elements are also small due to relations (29). $\tilde{S}_{h\hat{s}} \approx -\tilde{S}_{s\hat{h}}$ up to small corrections while $|\tilde{S}_{h\hat{H}}| < 0.1$ (< 0.01 in most cases). All these mixing elements are well below present experimental bounds. The numbers given in the table illustrate the expected order of magnitude for the soft mass parameters necessary to explain the di-photon excess in our scenario and indicate that it will be fine-tuned at the level of 1 per mille.

Finally we comment on the constraint from electroweak precision tests. It has been pointed out [95–97] that large values of λ and $\tan\beta$ may introduce a dangerous contribution from light

$\tan\beta$	$\lvert g_{Asa}\rvert$	$\tilde{S}_{s\hat{H}}$	λ	κ	A_λ [TeV]	μ' [TeV]	$m_h^{\rm tree}$ [GeV]	$\widetilde{m}_h$ [GeV]
2	2.1	0.15	1.38	-1.54	0.39	1.23	199	215
2	1.4	0.05	0.69	-2.04	0.41	2.63	110	112
2	1.0	0.09	0.79	-1.27	0.42	1.62	123	125
2	1.0	0.06	0.62	1.61	0.27	1.68	102	113
7	1.4	0.4	0.97	-1.57	0.87	2.07	100	112
20	1.3	0.5	0.80	-1.88	1.29	3.05	92	96
20	1.0	0.6	0.70	1.78	1.25	-0.65	92	95
20	0.6	0.6	0.51	1.46	1.79	-0.35	91	92

Table 1: Examples of solutions with vanishing $\tilde{S}_{s\hat{h}}$ and θ_{Aa} for $m_H = m_A = 850$ GeV, $m_s = 65$ GeV and $\mu = 375$ GeV. The SM-like Higgs boson mass at the tree level, $m_h^{\rm tree}$, and with the leading (for large λ and κ) loop corrections (but before including the radiative correction from the scalar top loop), $\widetilde{m}_h$, are given in the last two columns. Mixing elements $\tilde{S}_{h\hat{s}}$, $\tilde{S}_{h\hat{H}}$ and $\tilde{S}_{H\hat{h}}$ are at most of order 0.01 for all these examples.

higgsinos to the T-parameter [98] as a consequence of violation of SU(2) custodial symmetry. However, generically, in the selected region, $\lambda < 1$. Moreover, ref. [95] shows that even for $\lambda = 2$ there are strips around the singlino mass parameter $|\mu_s| = |\mu' + (\kappa/\lambda)\mu| \simeq 750 \div 800$ GeV where the higgsino contribution to the T-parameter vanishes or is negative independently of $\tan\beta$ and weakly dependent on the value of μ. It is not difficult to find solutions with the singlino mass in the above range, as for instance the last example in Table 1. We, therefore, expect the higgsino contribution to the T parameter not to be a problem for our scenario. One can also expect some cancellation between the higgsino contribution and the contributions from NMSSM Higgs bosons. We leave a detailed numerical analysis for future work.

4 Conclusions

We demonstrate that the plain NMSSM can explain the observed diphoton excess at $m_{\gamma\gamma} \simeq 750$ GeV as a decay of a single particle into two photons at the price of a relatively low UV cut-off (around 100 TeV) and of a certain fine tuning of the parameters. The mechanism behind this scenario is production of a doublet-like pseudo scalar A, decaying into a singlet-like pseudo scalar a, which subsequently decays via the vector-like higgsino loop into two photons. The predicted width of a is very small, much below the experimental resolution. The two-photon signal should be associated with b-quark jets coming from the decay $A \to as$, with s decaying dominantly into a pair of b quarks. The pseudo scalar a decays also into other channels with the branching ratios given by Eq. (5).

The topology proposed in this paper is the only one that can explain the 750 GeV excess in the plain NMSSM due to a single particle decay. Another possibility for the NMSSM, recently

proposed, is to explain the observed signal by the decays of two light pseudo scalars, to two collimated photons each. The latter interpretation could explain a broad peak at 750 GeV, if confirmed experimentally. The width of the signal will give a crucial discrimination between different proposed interpretations, in particular between perturbative and non-perturbative scenarios.

Acknowledgments We thank Michael Schmidt, Kai Schmidt-Hoberg and Florian Staub for valuable comments. MO and SP have been supported by the National Science Centre, Poland, under research grants DEC-2014/15/B/ST2/02157, DEC-2012/04/A/ST2/00099 and DEC-2015/18/M/ST2/00054. MB was supported in part by the Director, Office of Science, Office of High Energy and Nuclear Physics, of the US Department of Energy under Contract DE-AC02-05CH11231 and by the National Science Foundation under grant PHY-1316783. MB acknowledges support from the Polish Ministry of Science and Higher Education (decision no. 1266/MOB/IV/2015/0). SP and KS thank CERN Theory Division for its hospitality during the final work on this project.

References

[1] **ATLAS** Collaboration, *Search for resonances decaying to photon pairs in 3.2 fb^{-1} of pp collisions at $\sqrt{s}$ = 13 TeV with the ATLAS detector*, .

[2] **CMS** Collaboration, *Search for new physics in high mass diphoton events in proton-proton collisions at 13TeV*, .

[3] The ATLAS collaboration, *Search for resonances in diphoton events with the ATLAS detector at $\sqrt{s}$ = 13 TeV*, ATLAS-CONF-2016-018.

[4] **CMS** Collaboration, C. Collaboration, *Search for new physics in high mass diphoton events in* 3.3 fb^{-1} *of proton-proton collisions at* $\sqrt{s} = 13$ TeV *and combined interpretation of searches at* 8 TeV *and* 13 TeV, CMS-PAS-EXO-16-018.

[5] R. Franceschini, G. F. Giudice, J. F. Kamenik, M. McCullough, F. Riva, A. Strumia, and R. Torre, *Digamma, what next?*, 1604.06446.

[6] B. C. Allanach, P. S. B. Dev, S. A. Renner, and K. Sakurai, *Di-photon Excess Explained by a Resonant Sneutrino in R-parity Violating Supersymmetry*, 1512.07645.

[7] R. Ding, L. Huang, T. Li, and B. Zhu, *Interpreting* 750 *GeV Diphoton Excess with R-parity Violation Supersymmetry*, 1512.06560.

[8] U. Ellwanger and C. Hugonie, *A 750 GeV Diphoton Signal from a Very Light Pseudoscalar in the NMSSM*, 1602.03344.

[9] F. Domingo, S. Heinemeyer, J. S. Kim, and K. Rolbiecki, *The NMSSM lives - with the 750 GeV diphoton excess*, 1602.07691.

[10] R. Franceschini, G. F. Giudice, J. F. Kamenik, M. McCullough, A. Pomarol, R. Rattazzi, M. Redi, F. Riva, A. Strumia, and R. Torre, *What is the gamma gamma resonance at 750 GeV?*, 1512.04933.

[11] S. D. McDermott, P. Meade, and H. Ramani, *Singlet Scalar Resonances and the Diphoton Excess*, *Phys. Lett.* **B755** (2016) 353–357, [1512.05326].

[12] J. Ellis, S. A. R. Ellis, J. Quevillon, V. Sanz, and T. You, *On the Interpretation of a Possible ~ 750 GeV Particle Decaying into $\gamma\gamma$*, 1512.05327.

[13] R. S. Gupta, S. Jäger, Y. Kats, G. Perez, and E. Stamou, *Interpreting a 750 GeV Diphoton Resonance*, 1512.05332.

[14] R. Martinez, F. Ochoa, and C. F. Sierra, *Diphoton decay for a 750 GeV scalar boson in an $U(1)'$ model*, 1512.05617.

[15] S. Fichet, G. von Gersdorff, and C. Royon, *Scattering Light by Light at 750 GeV at the LHC*, 1512.05751.

[16] L. Bian, N. Chen, D. Liu, and J. Shu, *A hidden confining world on the 750 GeV diphoton excess*, 1512.05759.

[17] A. Falkowski, O. Slone, and T. Volansky, *Phenomenology of a 750 GeV Singlet*, *JHEP* **02** (2016) 152, [1512.05777].

[18] Y. Bai, J. Berger, and R. Lu, *A 750 GeV Dark Pion: Cousin of a Dark G-parity-odd WIMP*, 1512.05779.

[19] M. Dhuria and G. Goswami, *Perturbativity, vacuum stability and inflation in the light of 750 GeV diphoton excess*, 1512.06782.

[20] I. Chakraborty and A. Kundu, *Diphoton excess at 750 GeV: Singlet scalars confront triviality*, 1512.06508.

[21] F. Wang, L. Wu, J. M. Yang, and M. Zhang, *750 GeV Diphoton Resonance, 125 GeV Higgs and Muon g-2 Anomaly in Deflected Anomaly Mediation SUSY Breaking Scenario*, 1512.06715.

[22] A. E. C. Hernández and I. Nisandzic, *LHC diphoton 750 GeV resonance as an indication of $SU(3)_c \times SU(3)_L \times U(1)_X$ gauge symmetry*, 1512.07165.

[23] W.-C. Huang, Y.-L. S. Tsai, and T.-C. Yuan, *Gauged Two Higgs Doublet Model confronts the LHC 750 GeV di-photon anomaly*, 1512.07268.

[24] M. Badziak, *Interpreting the 750 GeV diphoton excess in minimal extensions of Two-Higgs-Doublet models*, 1512.07497.

[25] M. Cvetič, J. Halverson, and P. Langacker, *String Consistency, Heavy Exotics, and the 750 GeV Diphoton Excess at the LHC*, 1512.07622.

[26] K. Cheung, P. Ko, J. S. Lee, J. Park, and P.-Y. Tseng, *A Higgcision study on the 750 GeV Di-photon Resonance and 125 GeV SM Higgs boson with the Higgs-Singlet Mixing*, 1512.07853.

[27] J. Zhang and S. Zhou, *Electroweak Vacuum Stability and Diphoton Excess at 750 GeV*, 1512.07889.

[28] L. J. Hall, K. Harigaya, and Y. Nomura, *750 GeV Diphotons: Implications for Supersymmetric Unification*, 1512.07904.

[29] F. Wang, W. Wang, L. Wu, J. M. Yang, and M. Zhang, *Interpreting 750 GeV Diphoton Resonance in the NMSSM with Vector-like Particles*, 1512.08434.

[30] A. Salvio and A. Mazumdar, *Higgs Stability and the 750 GeV Diphoton Excess*, 1512.08184.

[31] M. Son and A. Urbano, *A new scalar resonance at 750 GeV: Towards a proof of concept in favor of strongly interacting theories*, 1512.08307.

[32] C. Cai, Z.-H. Yu, and H.-H. Zhang, *The 750 GeV diphoton resonance as a singlet scalar in an extra dimensional model*, 1512.08440.

[33] N. Bizot, S. Davidson, M. Frigerio, and J. L. Kneur, *Two Higgs doublets to explain the excesses $pp \to \gamma\gamma(750\text{ GeV})$ and $h \to \tau^{\pm}\mu^{\mp}$*, 1512.08508.

[34] Y. Hamada, T. Noumi, S. Sun, and G. Shiu, *An O(750) GeV Resonance and Inflation*, 1512.08984.

[35] S. K. Kang and J. Song, *Top-phobic heavy Higgs boson as the 750 GeV diphoton resonance*, 1512.08963.

[36] Y. Jiang, Y.-Y. Li, and T. Liu, *750 GeV Resonance in the Gauged $U(1)'$-Extended MSSM*, 1512.09127.

[37] S. Jung, J. Song, and Y. W. Yoon, *How Resonance-Continuum Interference Changes 750 GeV Diphoton Excess: Signal Enhancement and Peak Shift*, 1601.00006.

[38] J. Gu and Z. Liu, *Running after Diphoton*, 1512.07624.

[39] F. Goertz, J. F. Kamenik, A. Katz, and M. Nardecchia, *Indirect Constraints on the Scalar Di-Photon Resonance at the LHC*, 1512.08500.

[40] P. Ko, Y. Omura, and C. Yu, *Diphoton Excess at 750 GeV in leptophobic U(1)′ model inspired by E_6 GUT*, 1601.00586.

[41] E. Palti, *Vector-Like Exotics in F-Theory and 750 GeV Diphotons*, 1601.00285.

[42] A. Karozas, S. F. King, G. K. Leontaris, and A. K. Meadowcroft, *750 GeV Diphoton excess from E_6 in F-theory GUTs*, 1601.00640.

[43] S. Bhattacharya, S. Patra, N. Sahoo, and N. Sahu, *750 GeV Di-photon excess at CERN LHC from a dark sector assisted scalar decay*, 1601.01569.

[44] J. Cao, L. Shang, W. Su, Y. Zhang, and J. Zhu, *Interpreting the 750 GeV diphoton excess in the Minimal Dilaton Model*, 1601.02570.

[45] A. E. Faraggi and J. Rizos, *The 750 GeV diphoton LHC excess and Extra Z's in Heterotic-String Derived Models*, 1601.03604.

[46] X.-F. Han, L. Wang, and J. M. Yang, *An extension of two-Higgs-doublet model and the excesses of 750 GeV diphoton, muon g-2 and $h \to \mu\tau$*, 1601.04954.

[47] J. Kawamura and Y. Omura, *Diphoton excess at 750 GeV and LHC constraints in models with vector-like particles*, 1601.07396.

[48] S. F. King and R. Nevzorov, *750 GeV Diphoton Resonance from Singlets in an Exceptional Supersymmetric Standard Model*, 1601.07242.

[49] T. Nomura and H. Okada, *Generalized Zee-Babu model with 750 GeV Diphoton Resonance*, 1601.07339.

[50] K. Harigaya and Y. Nomura, *A Composite Model for the 750 GeV Diphoton Excess*, 1602.01092.

[51] C. Han, T. T. Yanagida, and N. Yokozaki, *Implications of the 750 GeV Diphoton Excess in Gaugino Mediation*, 1602.04204.

[52] Y. Hamada, H. Kawai, K. Kawana, and K. Tsumura, *Models of LHC Diphoton Excesses Valid up to the Planck scale*, 1602.04170.

[53] K. J. Bae, M. Endo, K. Hamaguchi, and T. Moroi, *Diphoton Excess and Running Couplings*, 1602.03653.

[54] A. Salvio, F. Staub, A. Strumia, and A. Urbano, *On the maximal diphoton width*, 1602.01460.

[55] R. Barbieri, D. Buttazzo, L. J. Hall, and D. Marzocca, *Higgs mass and unified gauge coupling in the NMSSM with Vector Matter*, 1603.00718.

[56] A. Pilaftsis, *Diphoton Signatures from Heavy Axion Decays at the CERN Large Hadron Collider*, *Phys. Rev.* **D93** (2016), no. 1 015017, [1512.04931].

[57] P. S. B. Dev and D. Teresi, *Asymmetric Dark Matter in the Sun and the Diphoton Excess at the LHC*, 1512.07243.

[58] P. S. B. Dev, R. N. Mohapatra, and Y. Zhang, *Quark Seesaw, Vectorlike Fermions and Diphoton Excess*, 1512.08507.

[59] C. Arbeláez, A. E. C. Hernández, S. Kovalenko, and I. Schmidt, *Linking radiative seesaw-type mechanism of fermion masses and non-trivial quark mixing with the 750 GeV diphoton excess*, 1602.03607.

[60] A. E. C. Hernández, I. d. M. Varzielas, and E. Schumacher, *The* 750 *GeV diphoton resonance in the light of a 2HDM with S_3 flavour symmetry*, 1601.00661.

[61] A. E. C. Hernández, *The 750 GeV diphoton resonance can cause the SM fermion mass and mixing pattern*, 1512.09092.

[62] S.-F. Ge, H.-J. He, J. Ren, and Z.-Z. Xianyu, *Realizing Dark Matter and Higgs Inflation in Light of LHC Diphoton Excess*, 1602.01801.

[63] W. Chao, *The Diphoton Excess Inspired Electroweak Baryogenesis*, 1601.04678.

[64] W. Chao, *The Diphoton Excess from an Exceptional Supersymmetric Standard Model*, 1601.00633.

[65] X.-F. Han and L. Wang, *Implication of the 750 GeV diphoton resonance on two-Higgs-doublet model and its extensions with Higgs field*, 1512.06587.

[66] X.-F. Han, L. Wang, L. Wu, J. M. Yang, and M. Zhang, *Explaining 750 GeV diphoton excess from top/bottom partner cascade decay in two-Higgs-doublet model extension*, 1601.00534.

[67] L. A. Anchordoqui, I. Antoniadis, H. Goldberg, X. Huang, D. Lust, and T. R. Taylor, *750 GeV diphotons from closed string states*, *Phys. Lett.* **B755** (2016) 312–315, [1512.08502].

[68] K. Harigaya and Y. Nomura, *Composite Models for the 750 GeV Diphoton Excess*, *Phys. Lett.* **B754** (2016) 151–156, [1512.04850].

[69] A. Djouadi, J. Ellis, and J. Quevillon, *Interference Effects in the Decays of 750 GeV States into $\gamma\gamma$ and $t\bar{t}$*, 1605.00542.

[70] A. Djouadi and A. Pilaftsis, *The 750 GeV Diphoton Resonance in the MSSM*, 1605.01040.

[71] A. Angelescu, A. Djouadi, and G. Moreau, *Scenarii for interpretations of the LHC diphoton excess: two Higgs doublets and vector-like quarks and leptons*, 1512.04921.

[72] F. P. Huang, C. S. Li, Z. L. Liu, and Y. Wang, *750 GeV Diphoton Excess from Cascade Decay*, 1512.06732.

[73] W. Altmannshofer, J. Galloway, S. Gori, A. L. Kagan, A. Martin, and J. Zupan, *On the 750 GeV di-photon excess*, 1512.07616.

[74] X.-J. Bi, R. Ding, Y. Fan, L. Huang, C. Li, T. Li, S. Raza, X.-C. Wang, and B. Zhu, *A Promising Interpretation of Diphoton Resonance at 750 GeV*, 1512.08497.

[75] R. Ding, Y. Fan, L. Huang, C. Li, T. Li, S. Raza, and B. Zhu, *Systematic Study of Diphoton Resonance at 750 GeV from Sgoldstino*, 1602.00977.

[76] R. V. Harlander, S. Liebler, and H. Mantler, *SusHi: A program for the calculation of Higgs production in gluon fusion and bottom-quark annihilation in the Standard Model and the MSSM*, *Comput. Phys. Commun.* **184** (2013) 1605–1617, [1212.3249].

[77] R. V. Harlander and W. B. Kilgore, *Higgs boson production in bottom quark fusion at next-to-next-to leading order*, *Phys. Rev.* **D68** (2003) 013001, [hep-ph/0304035].

[78] U. Aglietti, R. Bonciani, G. Degrassi, and A. Vicini, *Two loop light fermion contribution to Higgs production and decays*, *Phys. Lett.* **B595** (2004) 432–441, [hep-ph/0404071].

[79] R. Bonciani, G. Degrassi, and A. Vicini, *On the Generalized Harmonic Polylogarithms of One Complex Variable*, *Comput. Phys. Commun.* **182** (2011) 1253–1264, [1007.1891].

[80] G. Degrassi and P. Slavich, *NLO QCD bottom corrections to Higgs boson production in the MSSM*, *JHEP* **11** (2010) 044, [1007.3465].

[81] G. Degrassi, S. Di Vita, and P. Slavich, *NLO QCD corrections to pseudoscalar Higgs production in the MSSM*, *JHEP* **08** (2011) 128, [1107.0914].

[82] G. Degrassi, S. Di Vita, and P. Slavich, *On the NLO QCD Corrections to the Production of the Heaviest Neutral Higgs Scalar in the MSSM*, *Eur. Phys. J.* **C72** (2012) 2032, [1204.1016].

[83] R. Harlander and P. Kant, *Higgs production and decay: Analytic results at next-to-leading order QCD*, *JHEP* **12** (2005) 015, [hep-ph/0509189].

[84] **CMS** Collaboration, *Search for additional neutral Higgs bosons decaying to a pair of tau leptons in pp collisions at* $\sqrt{s}$ *= 7 and 8 TeV*, .

[85] K. Schmidt-Hoberg and F. Staub, *Enhanced $h \to \gamma\gamma$ rate in MSSM singlet extensions*, *JHEP* **10** (2012) 195, [1208.1683].

[86] U. Ellwanger, C. Hugonie, and A. M. Teixeira, *The Next-to-Minimal Supersymmetric Standard Model*, *Phys. Rept.* **496** (2010) 1–77, [0910.1785].

[87] H. M. Lee, S. Raby, M. Ratz, G. G. Ross, R. Schieren, K. Schmidt-Hoberg, and P. K. S. Vaudrevange, *Discrete R symmetries for the MSSM and its singlet extensions*, *Nucl. Phys.* **B850** (2011) 1–30, [1102.3595].

[88] G. G. Ross and K. Schmidt-Hoberg, *The Fine-Tuning of the Generalised NMSSM*, *Nucl. Phys.* **B862** (2012) 710–719, [1108.1284].

[89] **DELPHI, OPAL, ALEPH, LEP Working Group for Higgs Boson Searches, L3** Collaboration, S. Schael *et al.*, *Search for neutral MSSM Higgs bosons at LEP*, *Eur. Phys. J.* **C47** (2006) 547–587, [hep-ex/0602042].

[90] M. Badziak, M. Olechowski, and S. Pokorski, *New Regions in the NMSSM with a 125 GeV Higgs*, *JHEP* **1306** (2013) 043, [1304.5437].

[91] **ATLAS** Collaboration, G. Aad *et al.*, *Measurements of the Higgs boson production and decay rates and coupling strengths using pp collision data at $\sqrt{s} = 7$ and 8 TeV in the ATLAS experiment*, *Eur. Phys. J.* **C76** (2016), no. 1 6, [1507.04548].

[92] **CMS** Collaboration, V. Khachatryan *et al.*, *Precise determination of the mass of the Higgs boson and tests of compatibility of its couplings with the standard model predictions using proton collisions at 7 and 8 TeV*, *Eur. Phys. J.* **C75** (2015), no. 5 212, [1412.8662].

[93] U. Ellwanger and C. Hugonie, *Yukawa induced radiative corrections to the lightest Higgs boson mass in the NMSSM*, *Phys. Lett.* **B623** (2005) 93–103, [hep-ph/0504269].

[94] M. D. Goodsell, K. Nickel, and F. Staub, *Two-loop corrections to the Higgs masses in the NMSSM*, *Phys. Rev.* **D91** (2015) 035021, [1411.4665].

[95] R. Barbieri, L. J. Hall, Y. Nomura, and V. S. Rychkov, *Supersymmetry without a Light Higgs Boson*, *Phys. Rev.* **D75** (2007) 035007, [hep-ph/0607332].

[96] R. Franceschini and S. Gori, *Solving the μ problem with a heavy Higgs boson*, *JHEP* **05** (2011) 084, [1005.1070].

[97] T. Gherghetta, B. von Harling, A. D. Medina, and M. A. Schmidt, *The Scale-Invariant NMSSM and the 126 GeV Higgs Boson*, *JHEP* **02** (2013) 032, [1212.5243].

[98] M. E. Peskin and T. Takeuchi, *Estimation of oblique electroweak corrections*, *Phys. Rev.* **D46** (1992) 381–409.